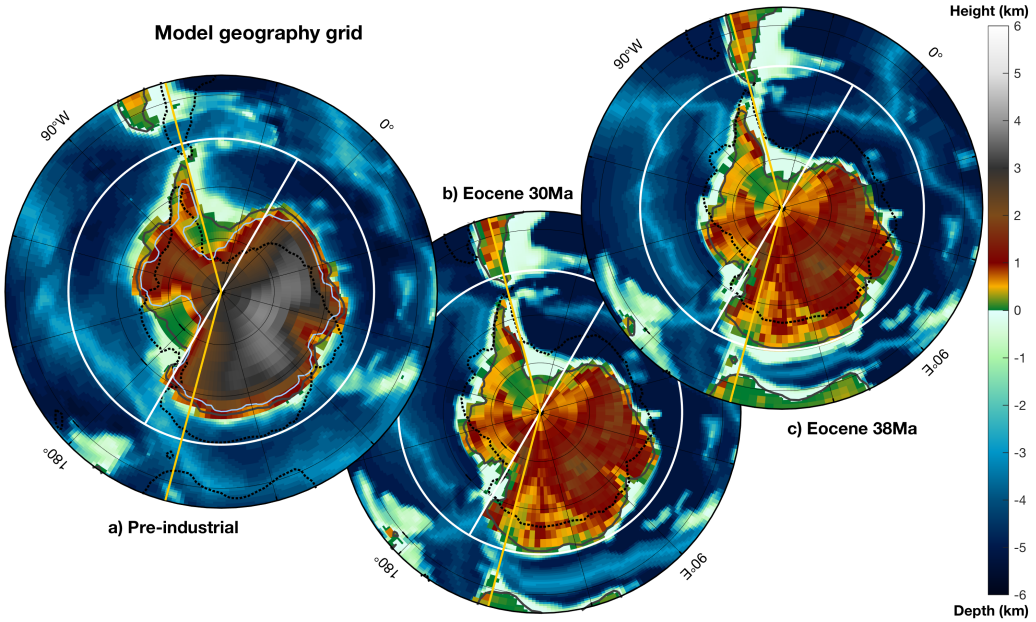

Figure S1: Antarctic geography comparison.
Antarctic model geography used in the **a)** pre-industrial, **b)** Eocene 30Ma, and **c)** Eocene 38Ma cases. Topography is shown using the atmospheric resolution, while bathymetry uses the oceanic model grid. Black dotted contours show the coastlines of alternate geographies for comparison; a) 38Ma Eocene, b) pre-industrial, and c) 30Ma Eocene. Yellow lines indicate the boundary used to make the cross sections in the atmosphere in Figure 4, the white semicircles show the same for the oceanic part.

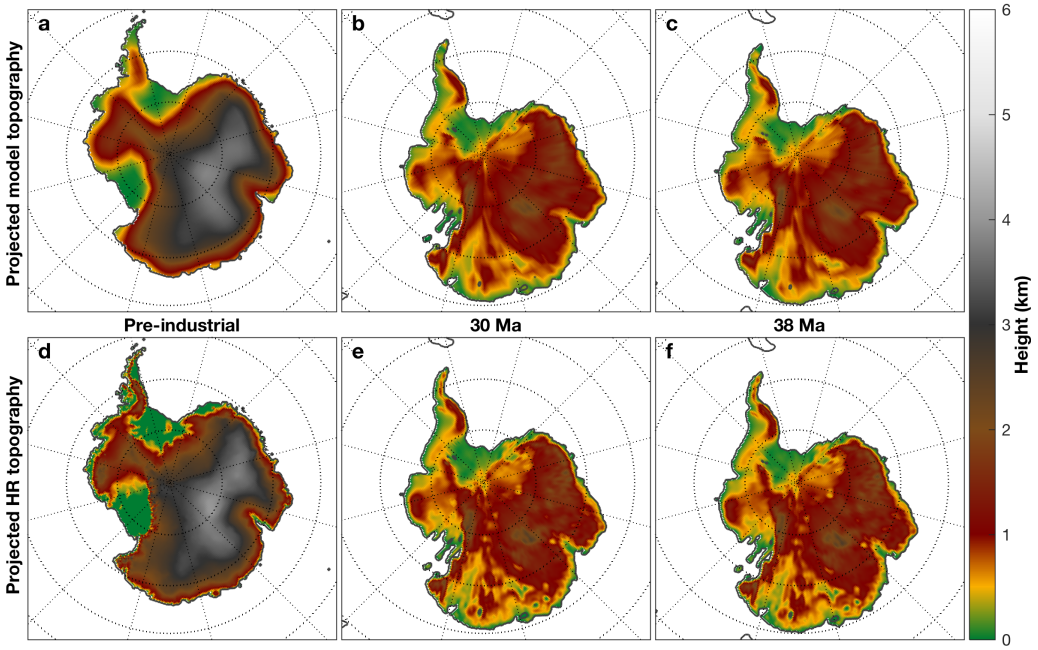

Figure S2: Comparison between model geography and high resolution reconstructions.
Rectangular polar stereographic projection of the Antarctic topography used in the different model cases (see Figure S1). Upper panels show the interpolated model geography, lower panels show the same for the original 0.25° reconstructions. The difference between the corresponding interpolations is used to adjust the temperature fields in the vegetation index calculations.

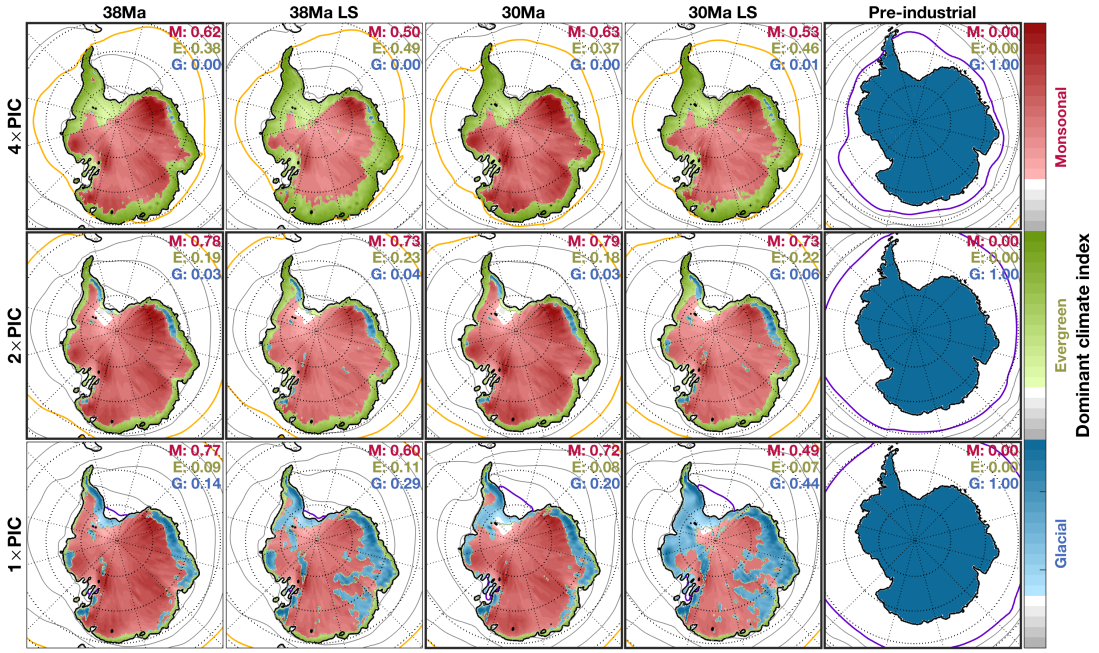

Figure S3: Overview of climate regimes.
Dominant climate index in the different simulated and extrapolated cases (LS: low summer insolation orbit; see also Table 1). Numbers show the fractional coverage across the Antarctic continent of each index. This supplementary figure is the equivalent of Figure 6, but rather using a continuous scale without any further division criteria.

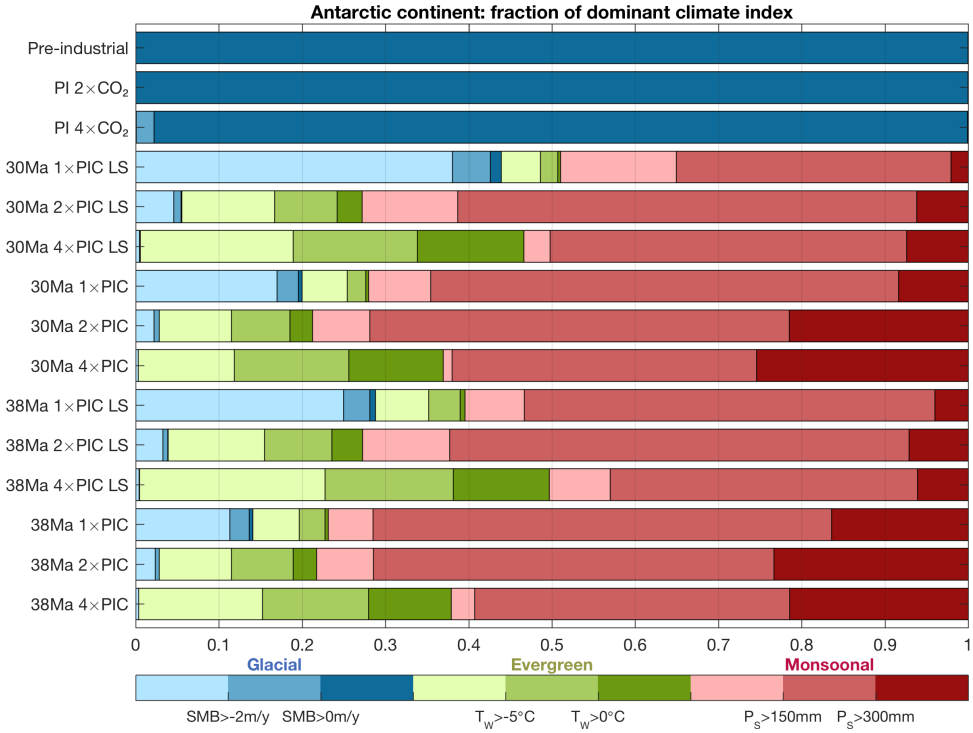

Figure S4: Dominant climate regime coverage.
Histogram showing the fractional areal extent of the dominant (i.e. largest at each grid cell) climate index for all of the considered scenarios. As in Figure 6, glacial index is subdivided by surface mass balance, evergreen vegetation by winter temperature, and monsoonal index by summer precipitation. An overview of the different case names and information can be found in Table 1.

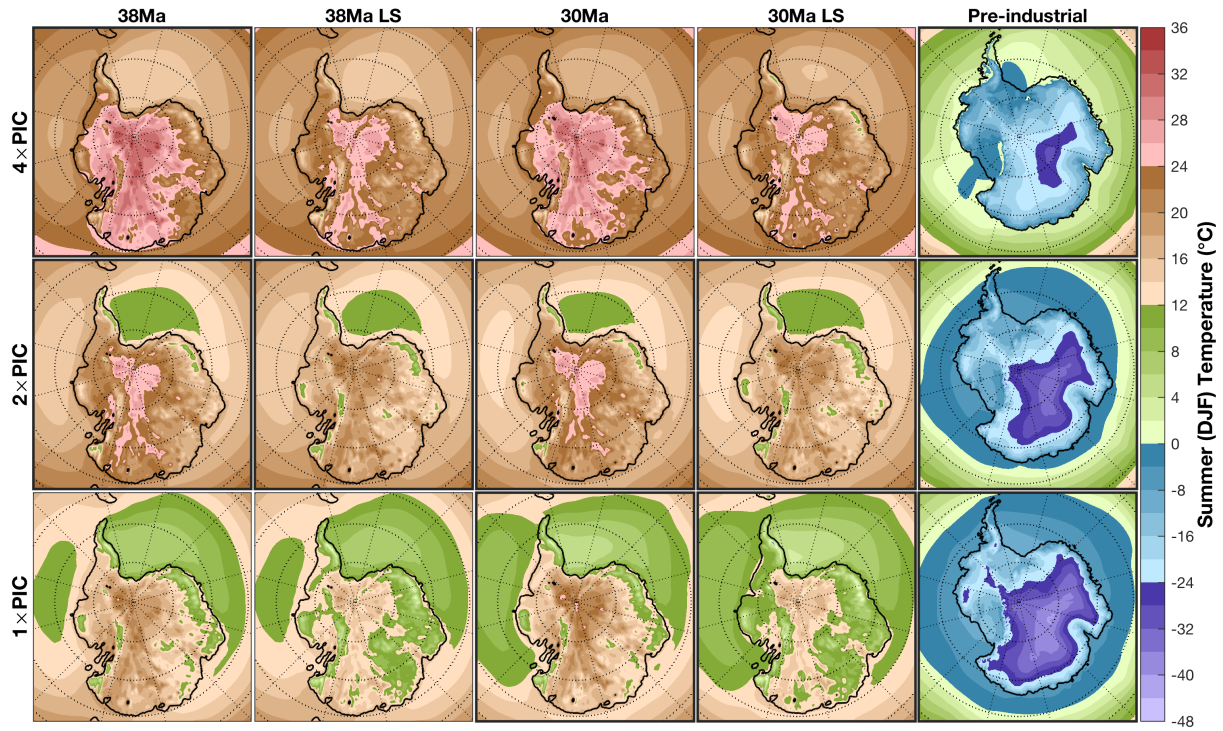

Figure S5: Antarctic summer temperature overview.
Polar stereographic view of interpolated and adjusted austral summer (DJF) mean temperature for all of the cases considered in this study.

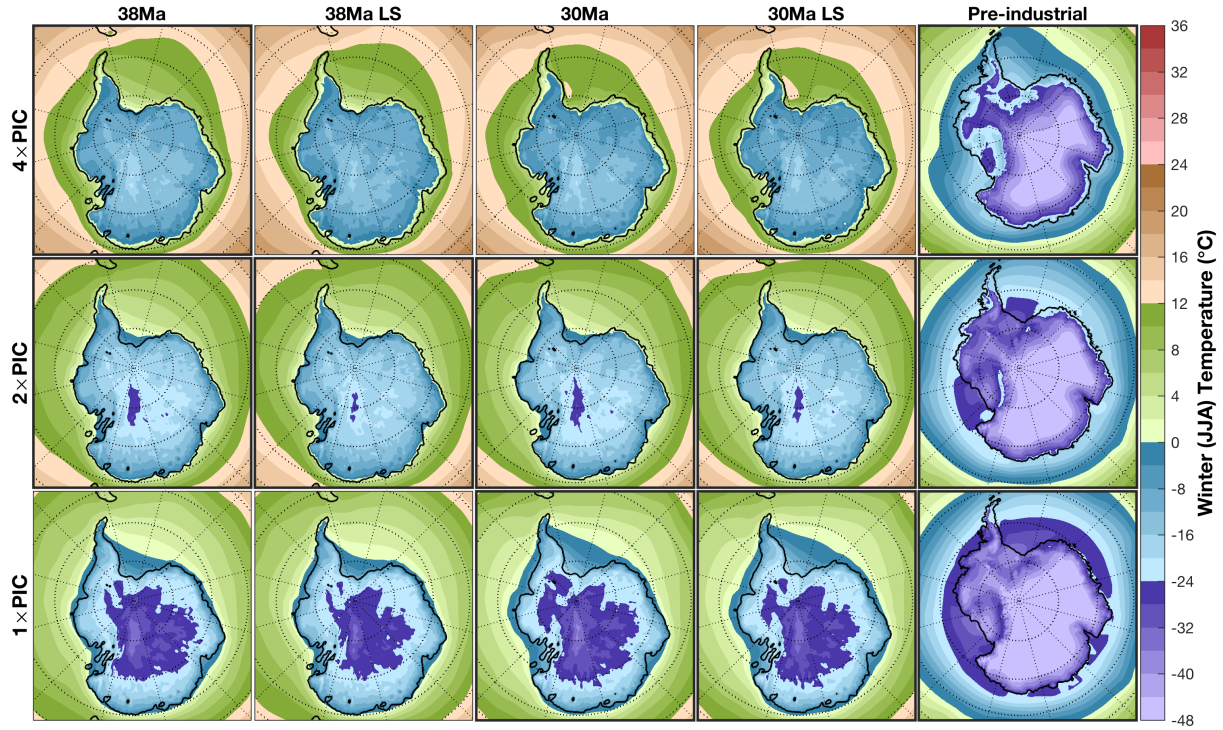

Figure S6: Antarctic winter temperature overview.
Polar stereographic view of interpolated and adjusted austral winter (JJA) mean temperature for all of the cases considered in this study.

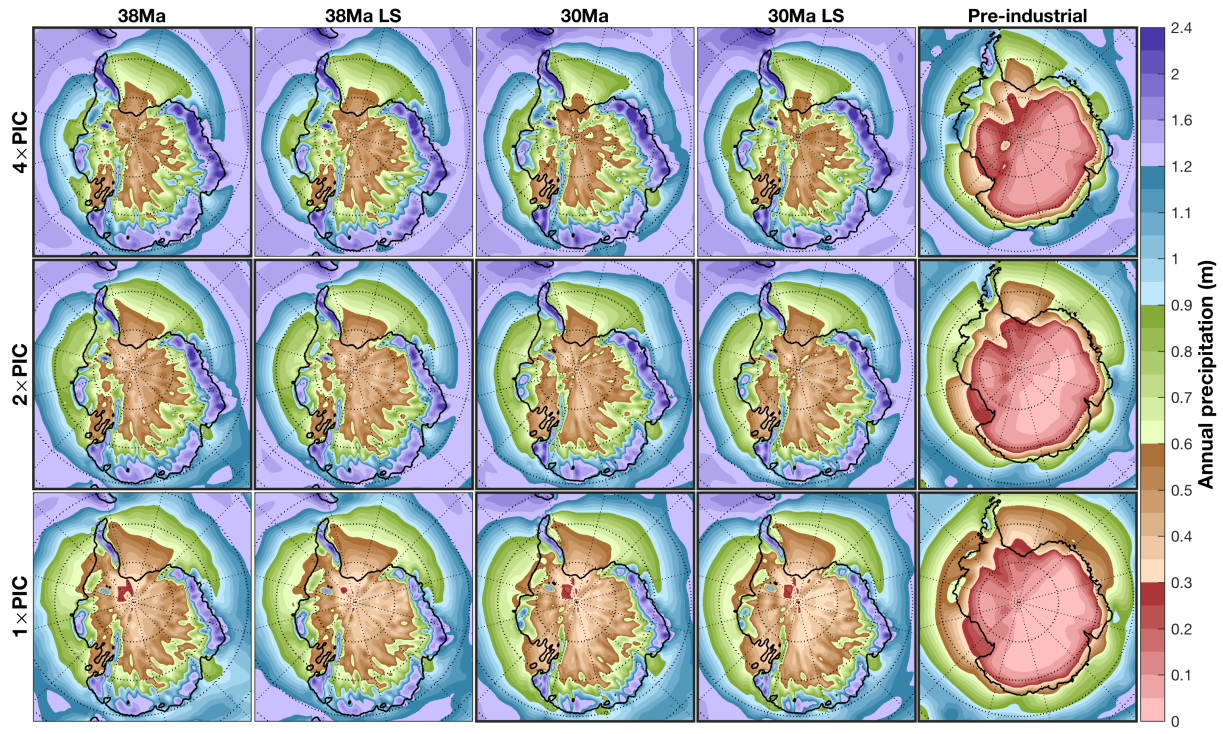

Figure S7: Antarctic annual precipitation overview.
Polar stereographic view of interpolated annual mean precipitation for all of the cases considered in this study.

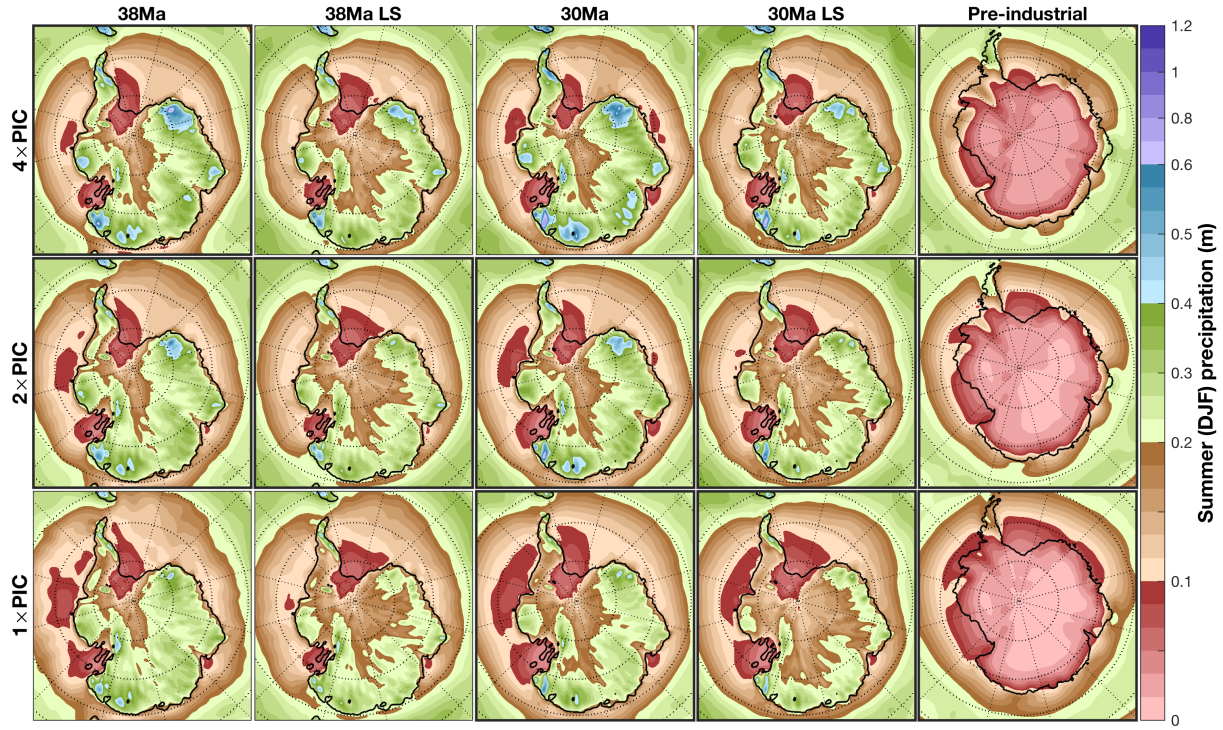

Figure S8: Antarctic summer precipitation overview.
Polar stereographic view of interpolated austral summer (DJF) mean precipitation for all of the cases considered in this study.

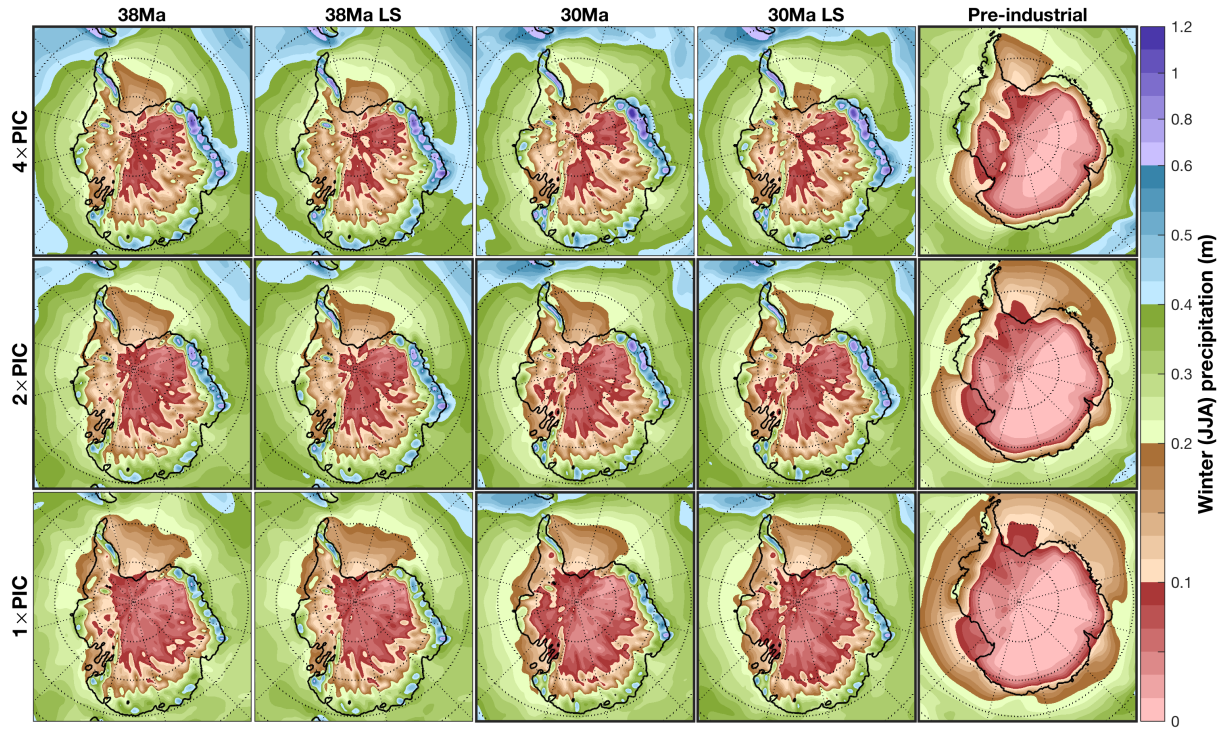

Figure S9: Antarctic winter precipitation overview.
Polar stereographic view of interpolated austral winter (JJA) mean precipitation for all of the cases considered in this study.

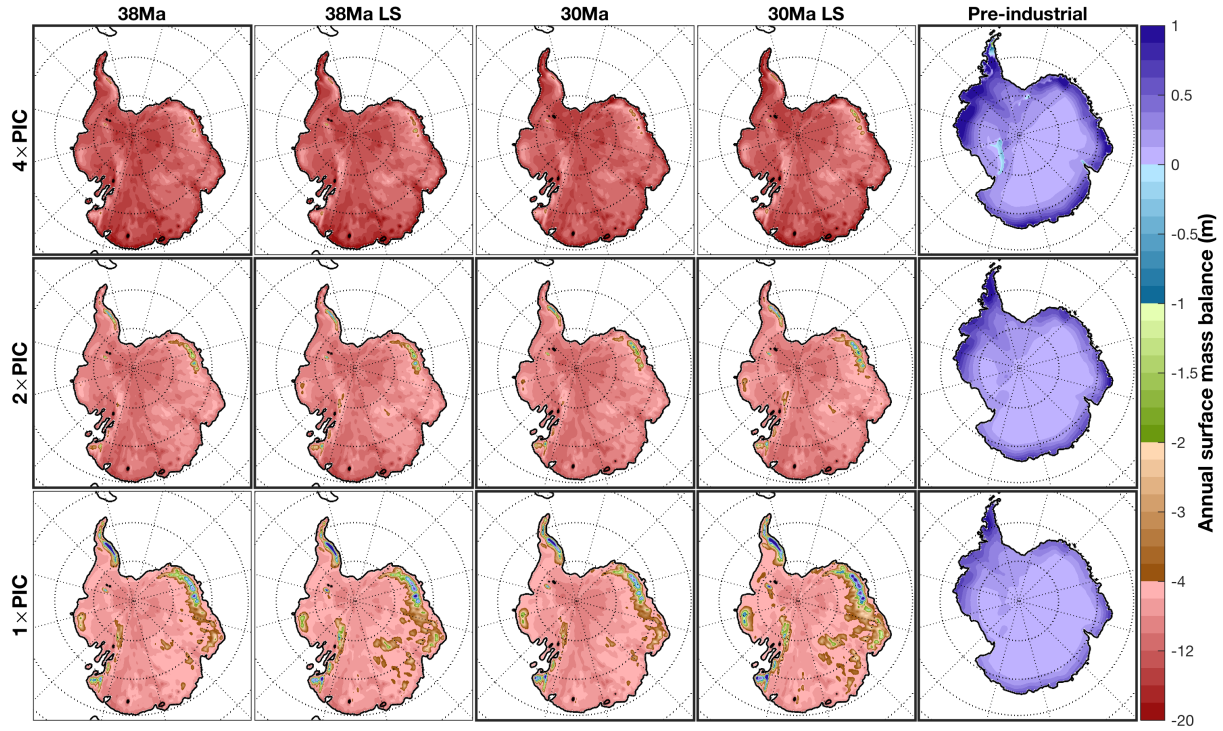

Figure S10: Antarctic annual surface mass balance overview.
Polar stereographic view of estimated annual surface mass balance for all of the cases considered in this study, using the respective interpolated and adjusted monthly climatologies of temperature and precipitation.

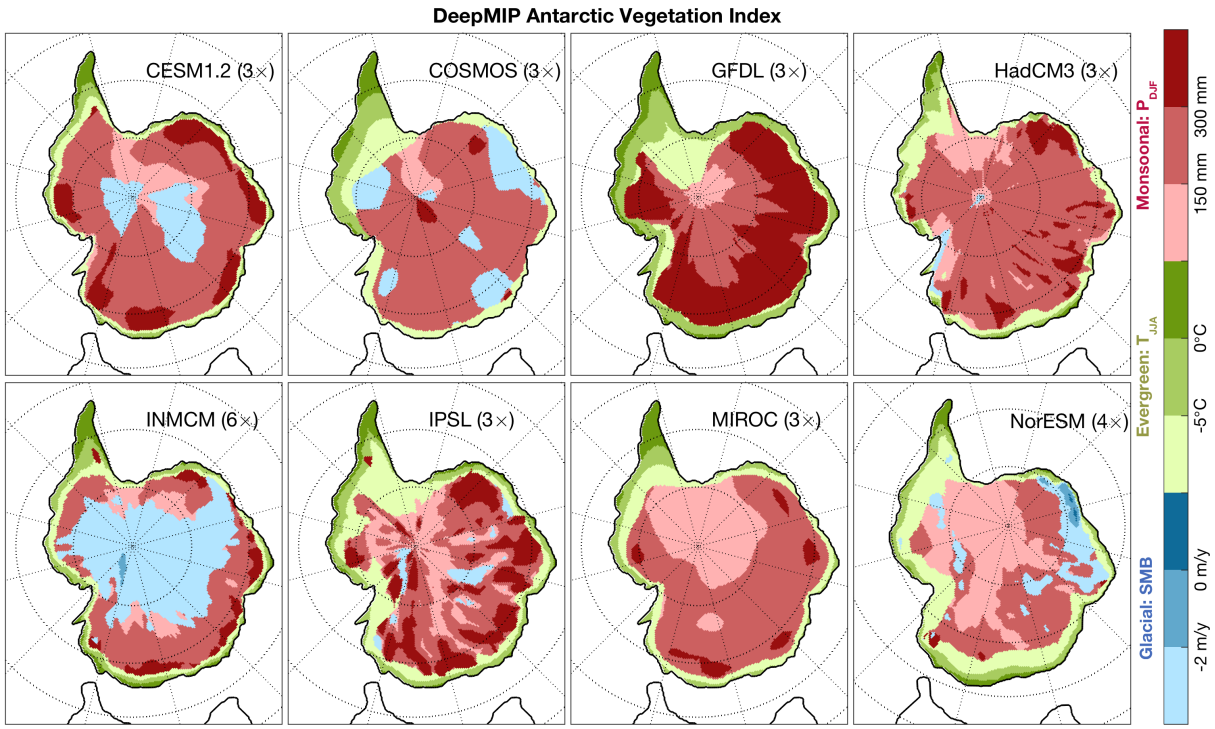

Figure S11: Comparison to DeepMIP.
Overview of climate index regimes in early Eocene simulations from DeepMIP, using their baseline with 3× pre-industrial CO_2 concentrations (6× in INMCM, 4× in NorESM; (*17, 20*)). The different indices are subdivided similarly to those in Figure 6.